Princeton Plasma Physics Laboratory

PPPL-5218

Phase space effects on fast ion distribution function modeling in tokamaks

M. Podesta , M. Gorelenkova, E. D. Fredrickson, N. N. Gorelenkov and R. B. White

December 2015

PRINCETON PLASMA PHYSICS LABORATORY

Prepared for the U.S. Department of Energy under Contract DE-AC02-09CH11466.

Phase space effects on fast ion distribution function modeling in tokamaks*

M. Podestà†‡, M. Gorelenkova, E. D. Fredrickson, N. N. Gorelenkov and R. B. White
Princeton Plasma Physics Laboratory, Princeton NJ 08543 - USA
(Dated: December 18, 2015)

Integrated simulations of tokamak discharges typically rely on *classical* physics to model energetic particle (EP) dynamics. However, there are numerous cases in which energetic particles can suffer additional transport that is not classical in nature. Examples include transport by applied 3D magnetic perturbations and, more notably, by plasma instabilities. Focusing on the effects of instabilities, *ad-hoc* models can empirically reproduce increased transport, but the choice of transport coefficients is usually somehow arbitrary. New approaches based on physics-based reduced models are being developed to address those issues in a simplified way, while retaining a more correct treatment of resonant wave-particle interactions. The *kick model* implemented in the tokamak transport code TRANSP is an example of such reduced models. It includes modifications of the EP distribution by instabilities in real and velocity space, retaining correlations between transport in energy and space typical of resonant EP transport. The relevance of EP phase space modifications by instabilities is first discussed in terms of predicted fast ion distribution. Results are compared with those from a simple, *ad-hoc* diffusive model. It is then shown that the phase-space resolved model can also provide additional insight into important issues such as internal consistency of the simulations and mode stability through the analysis of the power exchanged between energetic particles and the instabilities.

PACS numbers: 52.55.Fa, 52.35.Bj,52.55.Tn

I. INTRODUCTION

Burning fusion plasmas feature a high content of energetic particles (EP) originating from Neutral Beam (NB) injection, rf heating or fusion reactions [1]. Because of their crucial role, quantitative understanding and accurate modeling of the EP dynamics are required for interpreting present experiments and for predicting scenarios on future devices. Modeling tools already exist to model EP dynamic when energetic particles behave *classically*. Source and sink terms are well known and can be taken into account in the simulations with good accuracy. However, departure from classical behavior can be expected - and is indeed observed, cf. [2][3] and References therein - in the presence of perturbations of the EP evolution. The latter, for example, include magnetic perturbation induced by external coils, rf fields or plasma instabilities.

Several tools have been developed to study non-classical EP behavior, ranging from first-principles numerical codes [4][5][6][7][8][9] to reduced models [10][11][12][13] with various degree of simplifications. In particular, reduced models appear attractive for long time-scale integrated simulations of tokamak discharges, which typically require relatively short execution times to enable routine analysis of entire discharges or extensive parameter scans. This work focuses on the use of reduced models to include the effects of plasma instabilities (such as Alfvénic modes) in integrated simulations of tokamak discharges with energetic particles from Neutral Beam (NB) injection. Results from the NSTX device [14] will be discussed.

At a more fundamental level, the main goal of this work is to assess what level of complexity is required in modeling the evolution of the EP distribution function, F_{EP}, from which most of the other EP-related quantities are computed. For example, the latter include NB driven current and current drive efficiency, whose assessment is one of the major milestones for the NSTX Upgrade device [15]. Results from two EP transport models are compared. The main difference between the two models is whether EP transport is simply assumed to occur as diffusion the radial coordinate, or modifications of particle's *phase space* are also imodeled.

The following Sections include an introduction to the main modeling tools used in this work (Sec. II), followed by a description of the experimental scenario on which simulations are based upon (Sec. III). Section IV contains the main results of this work, starting with examples of EP distributions obtained from the two models. The implications of the differences in EP distribution from the two models on the consistency of the simulations are then discussed. As an example, the power balance between energetic ions and the instabilities they drive is taken as figure of merit to assess the consistency of the simulations. Section V summarizes the main findings of this work and concludes the paper.

II. MODELING TOOLS

The main tool used in this work for integrated tokamak modeling is the TRANSP code [16][17]. Energetic particle evolution is modeled through the NUBEAM module [18][19] of TRANSP, which includes several models

*Paper NI3-6, *Bull. Am. Phys. Soc.* **60** 216 (2015)
†Invited speaker
‡email: mpodesta@pppl.gov

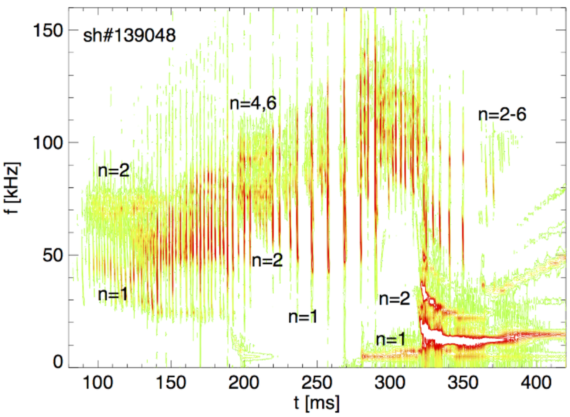

FIG. 1: Frequency spectrum of magnetic fluctuatens from Mirnov coils installed at the low-field side vessel awl for NSTX discharge #139048. Toroidal mode numbers of the different instabilities are indicated in the figure.

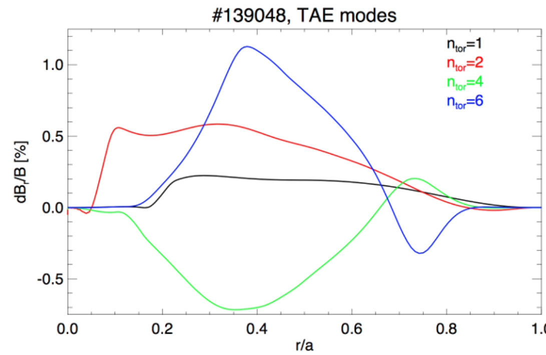

FIG. 2: Radial mode structure computed by the NOVA code for the $n_{tor} = 1-6$ TAE modes observed in Fig. 1 for $t \gtrsim 200$ ms. Note the radial extension of the modes, covering the entire minor radius. The amplitude of the radial magnetic field perturbation, $\delta B_r/B$, corresponds to a normalized mode amplitude $A_{mode} = 1$ for the kick model.

for additional EP transport in addition to classical EP physics. For simplicity, results presented here are limited to the two models described below.

The first model is based on the simplest possible assumption of purely diffusive EP transport, with a particle flux given by

$$\Gamma_{nb} = -D_b \nabla n_b \tag{1}$$

where ∇n_b is the radial gradient of the beam ion density. The diffusion coefficient D_b in Eq. 1 is an *ad-hoc* parameter, here assumed to be uniform in radius and with no energy dependence. D_b values are chosen to match measured quantities such as the neutron rate (see below). A time dependence $D_b = D_b(t)$ can be retained to improve the match with the experimental data as a function of time. Typical values are $0 \leq D_b \leq 5\ m^2/s$.

The second model (referred to as kick model) is based on a transport probability $p(\Delta E, \Delta P_\zeta | E, P_\zeta, \mu)$, which describes changes in particle's energy and toroidal canonical momentum resulting from the instabilities [20]. The transport matrix is pre-calculated through particle-following codes such as ORBIT [21], using perturbations modeled by MHD codes such as NOVA [22][23][24] that reproduce experimentally observed instabilities in terms of frequency and mode number spectrum. In practice, during a TRANSP run particles are classified based on their phase space variables E, P_ζ and μ, which indicate energy, toroidal canonical momentum and magnetic moment according to the normalizations used in [25]. As time evolves, particles experience kicks ΔE, ΔP_ζ according to the probability matrix, based on their phase space location. This probabilistic approach naturally fits with the MonteCarlo approach on which the NUBEAM module is based. Up to 10 probability matrices can be provided as input to model different modes, or sets of modes with similar properties. Free parameters for simulations with the kick model are the mode amplitudes as a function of time. Amplitudes are inferred from experimental measurements, when available. Further iterations may be required to achieve a better agreement with the measured neutron rate and stored energy. More details on the model can be found in Ref. [20].

III. EXPERIMENTAL SCENARIO

Results presented in this work refer to NSTX discharge #139048. Plasma current reaches its stationary level of 0.9 MA at ~ 200 ms. Toroidal field on axis is 0.45 T. Up to 6 MW of NB power are injected, with increasing steps of 2 MW between 50 ms and 200 ms. The discharge transitions into H-mode confinement during the current ramp-up phase and stays in H-mode until its termination.

As shown in Fig. 1, a rich variety of Alfvènic activity is observed throughout the discharge. Reverse-shear AEs with low toroidal mode number, $n = 1-2$, are present during the current ramp-up. Afterwards, toroidal AEs (TAEs) with $n = 1-6$ become dominant. Alfvènic instabilities co-exist with lower frequency, kink-like modes as the minimum of the safety factor approaches $q_{min} \sim 1$ for $t \geq 320$ ms. As typical for strongly NB-driven NSTX discharges, higher frequency Global and Compressional AEs are also measured at frequencies $\gg 200$ kHz [26]. Those modes will not be considered in the following analysis.

Instabilities in the TAE frequency range have been analyzed through the ideal MHD code NOVA [22][23][24] to infer the radial mode structure, based on the comparison with experimental data from Mirnov coils and a multi-channel reflectometer array [27][28]. The complete analysis is described in Ref. [29]. The inferred radial mode structures for TAEs with toroidal mode number $n_{tor} = 1, 2, 4, 6$ are shown in Fig. 2. Modes cover most of the minor radius, which is typical for TAEs observed on NSTX [29][30].

No experimental data is available for the mode structure of the kink-like modes. Therefore, a simple analyti-

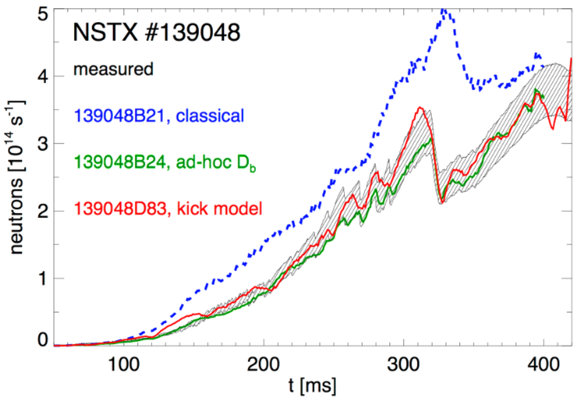

FIG. 3: Neutron rate for NSTX discharge #139048. Dashed region indicates the measured values, assuming a ±5 % uncertainty in the measurements. Dashed line is the predicted neutron rate from TRANSP assuming classical fast ion physics.. Solid lines are the results with enhanced fast ion transport using the ad-hoc D_b and kick models.

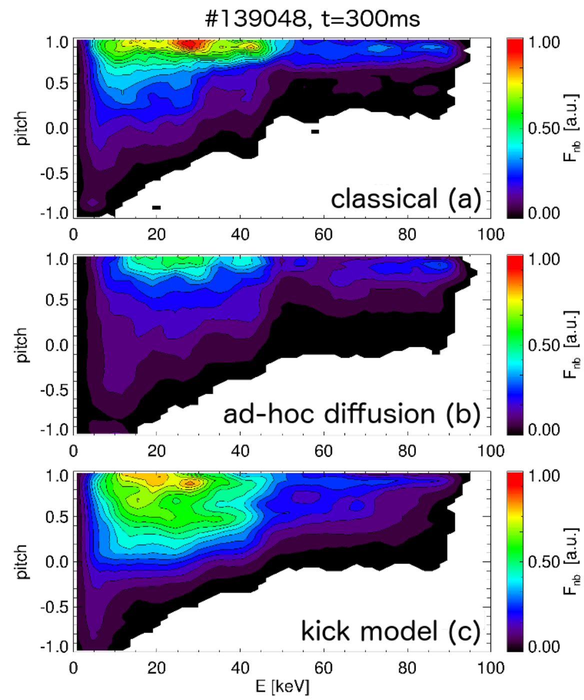

FIG. 4: Fast ion distribution computed by NUBEAM at $t \approx 300$ ms assuming classical fast ion physics and enhanced transport through the ad-hoc D_b and kick models. Normalization factor is the same for all distributions.

cal model is used to model their structure [31].

Data from magnetic pick-up coils installed at the low-field side plasma wall are used in the following to infer the temporal evolution of the mode amplitude for each of the modes shown in Figs. 1-2.

IV. MODELING RESULTS

TRANSP runs based on the same experimental profiles for NSTX discharge #139048 and different assumptions on fast ion transport provide the main results for the following analysis. Runs assuming *classical* transport are used as reference and set an upper limit for quantities such as fast ion density, neutron rate and stored energy in the absence of enhanced EP transport. Runs with the *ad-hoc* diffusive model and the *kick* model are iterated until satisfactory agreement between simulated and measured neutron rate is achieved, see Fig. 3. Free parameters for the two models are the assumed D_b and mode amplitude, respectively.

A. EP distribution function

A first comparison for the fast ion distribution as function of energy and pitch ($p \equiv v_\parallel/v$, ratio of parallel to total fast ion velocity) is shown in Fig. 4. NB injection energy is $E_0 = 90$ keV in the co-current direction, with about 50% of the injected neutrals populating the $E_0/2$ and $E_0/3$ energy components. After the injected neutrals are ionized, the resulting fast ions slow down in energy and spread in pitch until they are either lost or thermalized.

The addition of enhanced radial diffusivity causes a net depletion in the fast ion population, which appears in the energetic particle distribution function F_{EP} as an overall reduction over the entire energy and pitch range (Fig. 4b). If phase space modifications are then introduced through the kick model, more significant differences from the classical case arise (Fig. 4c). The distribution broadens significantly at lower energies for instabilities that mainly act on strongly co-passing particles with pitch $p \sim 1$. This populates regions that are otherwise poorly populated, such as trapped and stagnation orbits around $p \sim 0$.

From analysis with the ORBIT code, TAE modes observed in NSTX discharge #139048 have stronger resonances with co-passing fast ions. For example, Fig. 5 illustrates the kick probability $p(\Delta E, \Delta P_\zeta)$ resulting from the $n_{tor} = 4$ perturbation shown in Fig. 2 for ions with energy 75 keV. Resonant wave-particle interactions have increasingly stronger effects as $\mu \to 0$, corresponding to $|p| \to 1$ (i.e., strongly co- or counter-passing particles). Almost no interaction occurs for trapped particles.

The relative change in F_{EP} as predicted by the two models is shown in Fig. 6. The ad-hoc diffusivity pushes particles over a broad range of pitch, from regions populated by NB injection at $p > 0.6$ towards regions of the (E, p) space where no particles are observed in the classical run (cf. Fig. 4a). The kick model leads to more localized depletion around the injection pitch. The region $p < 0.4$ seems unaffected by the enhanced transport, and features a larger increase than in the case of enhanced D_b. For both cases, a broad energy range is affected. This is intrinsic in the ad-hoc diffusivity model, which has no

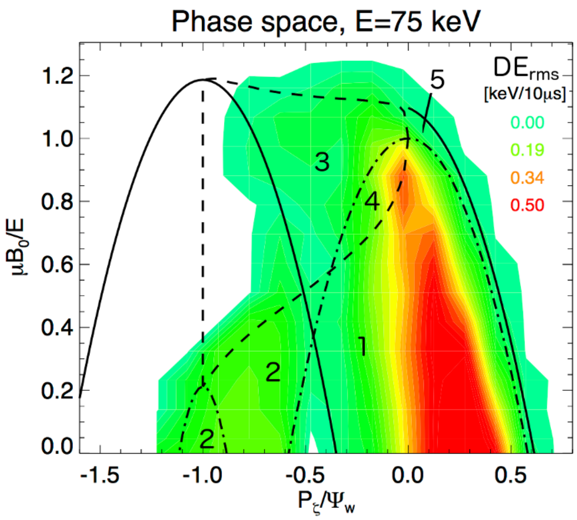

FIG. 5: Example of phase space for $E = 75$ keV fast ions for NSTX discharge #139048 at $t \approx 300$ ms. Regions correspond to (1) co-passing, (2) counter-passing, (3) trapped, (4) potato and (5) stagnation orbits [25]. Colored regions indicate the root-mean-square energy kicks, ΔE_{rms}, computed by ORBIT for a $n_{tor} = 4$ TAE mode.

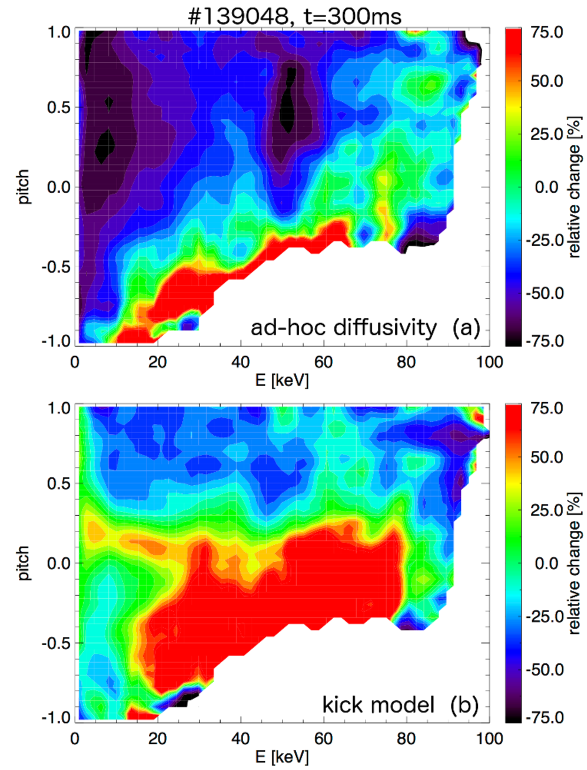

FIG. 6: Relative change of the fast ion distribution function (same shown in Fig. 4) caused by instabilities. Fast ion transport is computed using (a) ad-hoc D_b model and (b) kick model.

energy discrimination in its implementation used in this work. For the kick model, this is a result of the large number of resonances from multiple modes that form a dense net in phase space [32].

Additional details on the changes in distribution function from the three runs are presented in Fig. 7. F_{EP} modifications remain small at energies $E \approx 80$ keV, near the injection energy. Here the EP population is continuously replenished by NB injection, and the source term dominates in the distribution function evolution. At lower energy, $E \approx 20$ keV, significant differences in the temporal evolution of F_{EP} are apparent from the departure of average pitch and its broadening with respect to classical simulations.

The ad-hoc D_b and kick models differ in predicting the average pitch and the width of the distribution (here quantified as broadening in pitch). Moreover, the kick model shows larger variability in time, depending on the mix and relative amplitude of the modes included in the computation of the kick probability matrix at each specific time.

B. Integrals of F_{EP}: fast ion density, losses and NB power to thermal plasma

The effects of modifications of F_{EP} and its temporal evolution propagate to other quantities in whole-discharge simulations, as can be appreciated from Fig. 8. The depletion of the distribution function caused by enhanced transport directly transfers to a reduction in the fast ion density, n_b, obtained by integrating F_{EP} over phase space. The radial density gradient also decreases, indicating a flattening of the radial fast ion profile (Fig. 8a). A significant flattening with respect to classical simulations is predicted by both transport models, with shorter time-scale variations resulting from the kick model in response to spikes of the mode amplitude.

Reduced density is accompanied by enhanced EP losses from the core plasma, see Fig. 8b. The two models predict comparable losses during the initial ≈ 200 ms of the discharge. Mode activity is dominated by $n = 1, 2$ AEs in the kick model during this time. After $t \approx 200$ ms, direct losses computed using the kick model gradually decrease toward the classical level. In this case, transport in phase space mainly results in energy redistribution to lower energies and in enhanced charge-exchange losses for particles orbiting through the plasma edge. The ad-hoc diffusive model lacks of energy dependence for D_b, and therefore the only channel for transport is to increase the losses from the plasma. This is visible from the large spikes in fast ion losses in Fig. 8b.

Fast ions that are not lost during slowing-down will eventually transfer power to the thermal plasma and thermalize. Focusing on the NB power transferred to the electrons, see Fig. 8c, results are comparable for the two models. Consistently with the reduced loss rate from Fig. 8b, the kick model predicts a slightly larger power transferred to the electrons after $t \approx 250$ ms than the ad-hoc diffusive model. Although the difference may appear

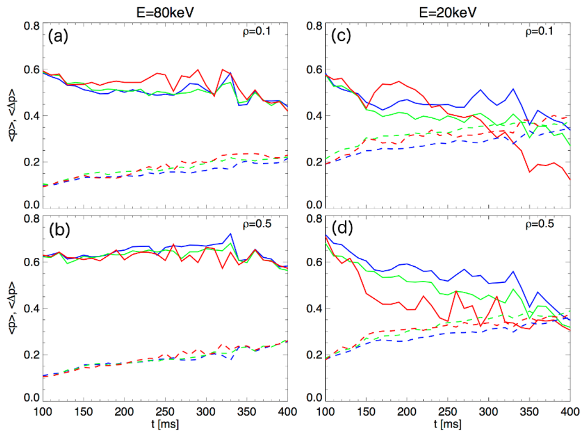

FIG. 7: Time evolution of the average pitch, $< p >$ (solid lines), and average pitch broadening, $< \Delta p >$ (dashed lines). Colors refer to classical runs (blue) and enhanced fast ion transport using the ad-hoc D_b (green) or kick (red) models. Panels refer to (a-b) $75 < E < 85$ keV fast ions and (c-d) $15 < E < 25$ keV fast ions at two different normalized radii, $\rho = 0.1$ and $\rho = 0.5$.

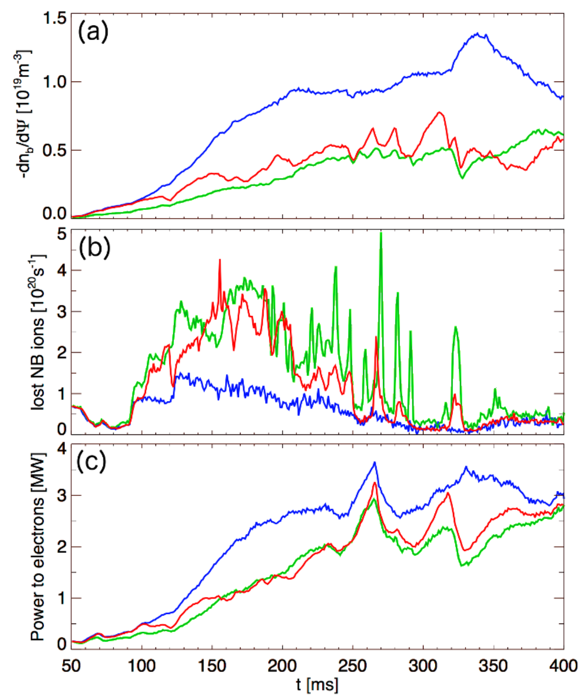

FIG. 8: (a) Radial gradient of the fast ion profile around $\rho = 0.5$ for classical simulations (blue) and assuming enhanced transport through ad-hoc diffusivity (green) and kick model (red). (b) Total fast ion loss rate for the three cases. (c) Total fast ion power damped on the thermal electrons through slowing-down.

small, it can still have a significant impact on power balance and thermal transport analyses based on TRANSP results, since local values as a function of radius can vary substantially [33].

To conclude this Section, there is evidence that the use of a specific transport model can result in significant differences for the predicted fast ion distribution function. Those differences can propagate to integral quantities such as EP radial density profile and loss rate. More subtle variations can also result from the models, such as NB power transfer to the thermal plasma and its radial deposition profile. (More example of integral quantities computed through the ad-hoc D_b vs kick model can be found in a separate work, cf. Ref. [33]). The following Section shows how the additional information made available by the phase space-resolved transport model can be a powerful tool to assess the consistency of the underlying EP transport assumptions. New physics insight can also be gained, for example, on the instabilities causing the enhanced transport.

C. Consistency of the results from AE power balance analysis

Consider a mode interacting resonantly with some portion of the EP distribution function. For the mode to be unstable, a net positive power must be transferred from the interacting fast ions to the mode, causing the mode amplitude to increase. A simple expression for the time evolution of the mode energy, E_w, is

$$\frac{\partial E_w}{\partial t} = P_{EP} - 2\gamma_{damp} E_w \tag{2}$$

where P_{EP} is the power from the fast ions to the mode and γ_{damp} the mode's damping rate.

At small mode amplitude (proportional to $\sqrt{E_w}$), the feedback of the mode on the EP distribution is negligible, so that $P_{EP} \approx constant$ and E_w grows exponentially in time. After this initial linear phase, the mode starts to affect the region of phase space in which interaction occurs, pushing particles outside that region. This implies that P_{EP} (which is now a function of E_w, in this non-linear phase) decreases, eventually leading to saturation with $E_w \approx P_{EP}(E_w)/2\gamma_{damp}$.

The mode evolution for a real case can be more complicated. Each mode can interact with multiple phase space regions, since several resonances can be present even for a single mode. In addition, P_{EP} also depends on EP sources (e.g. from NB injection and EP slowing down) that replenish the fast ion distribution regions depleted by the interaction with the mode. Moreover, the mode damping rate γ_{damp} can vary in time. All this leads to a dynamical balance between mode drive and damping, whether the latter is through damping on the thermal plasma or effective damping by depletion of particles in the resonant phase space regions.

Given all the complications that are present in a real case, it seems plausible to assume that a necessary condition for a mode to be unstable and to reach saturation

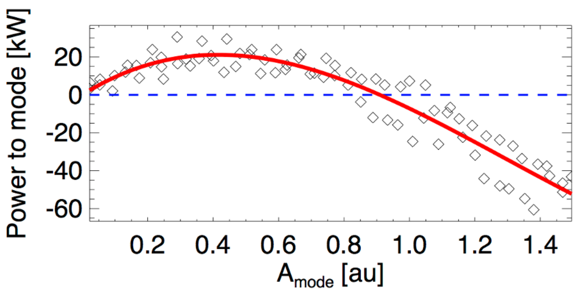

FIG. 9: Example of power transferred from the fast ions to a $n_{tor} = 4$ TAE mode, as computed by the kick model. Mode amplitude is swept with a triangular waveform for $0 \leq A_{mode} \leq 1.5$. Note the initial increase and successive roll-off of $P_{EP,j}(A_{mode})$, eventually leading to a *negative* power when the mode amplitude exceeds the inferred saturation amplitude, $A^{sat}_{mode} \approx 0.9$ in normalized units.

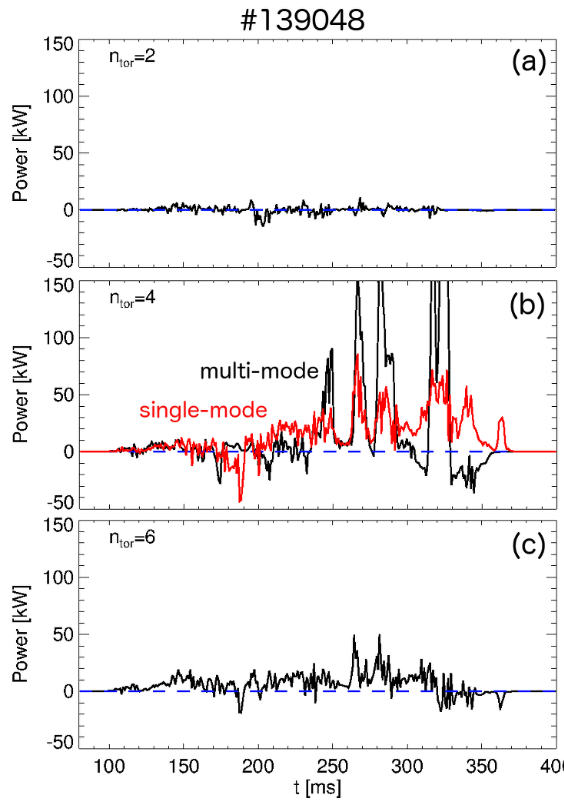

FIG. 10: Power $P_{EP,j}$ from fast ions to TAE modes with $n_{tor} = 2, 4, 6$ computed by the kick model. Panel (b) shows a comparison of $P_{EP,j}$ from multi-mode vs. single-mode simulations.

is given by

$$P_{EP}(E_w) \gtrsim 0 \quad for\, E_w > 0 \tag{3}$$

where $P_{EP}(E_w) \approx 0$ for finite E_w is the minimal condition in the limit $\gamma_{damp} \to 0$. (A finite γ_{damp} will increase the power P_{EP} required to sustain a finite mode amplitude).

The kick model does compute the power $P_{EP,j}$ exchanged between fast ions and each of the $j = 1 \dots N$ modes provided as input. An example is shown in Fig. 9 for the $n_{tor} = 4$ TAE mode shown in Fig. 2. To produce those data, the (normalized) mode amplitude was scanned in the range $0 \leq A_{mode}(t) \leq 1.5$ with a triangular waveform over time windows of ~ 50 ms. Note the roll-over of P_{EP} as the amplitude is increased above $A_{mode} \approx 0.5$. Eventually, P_{EP} becomes negative indicating that the un-physical condition for which the mode *transfers* power back into the EP population is achieved. For this example, the saturation amplitude would then be $A_{mode} \approx 0.9$ assuming $\gamma_{damp} = 0$.

Combined with the condition in Eq. 3, the knowledge of $P_{EP,j}(t)$ provides a powerful tool to verify that the assumptions made in the kick model (e.g. mode amplitude, kick probability) are indeed consistent with the modeled F_{EP} evolution. The computed values of $P_{EP,j}$ for the dominant $n_{tor} = 2, 4, 6$ TAEs used in the simulations discussed in the previous Sections are shown in Fig. 10. A first observation is that *dominant* modes can be identified. In this case, the $n_{tor} = 4$ TAE accounts for most of the fast ion power going to the modes, followed by the $n_{tor} = 6$ mode. The contribution of the $n_{tor} = 2$ mode appears negligible. Overall, all three modes are characterized by a net positive power, except for short time windows. This indicates that their mode structure and amplitude, combined with the calculated kick probabilities $p(\Delta E, \Delta P_\zeta)$, are consistent with the modeled scenario.

It is important to note that consistency encompasses all the modes, rather than a single mode. For example, Fig. 10b compares the values of $P_{EP,j}$ for the same $n_{tor} = 4$ mode when all other modes are included (referred to as *multi-mode* case) with values obtained excluding the other modes (*single-mode* case), i.e. A_{mode} is set to 0 for all other modes. It can be seen that $P_{EP,j}$ varies considerably for the two cases, which indicates that there exist mutual effects between the selected modes. This can be understood in terms of phase-space overlap of resonances from different modes, which cause instabilities to interact with the same groups of particles. The effects are not negligible and can result in significant variations in the computed profiles. Figure 11 shows the radial fast ion profiles at two different times for the multi- and single-mode cases. When only the $n_{tor} = 4$ TAE is retained, depletion in the fast ion density is much reduced. In some cases (e.g. at $t \approx 190$ ms in the figure) the absence of other instabilities causes $P_{EP,j}$ to become negative, which results in an unphysical steepening of the profile. Removing the synergy with the other TAEs, the $n_{tor} = 4$ mode would therefore be *stable* at that time.

V. SUMMARY AND CONCLUSIONS

Results on EP distribution function predictions through integrated simulations from two fast ion trans-

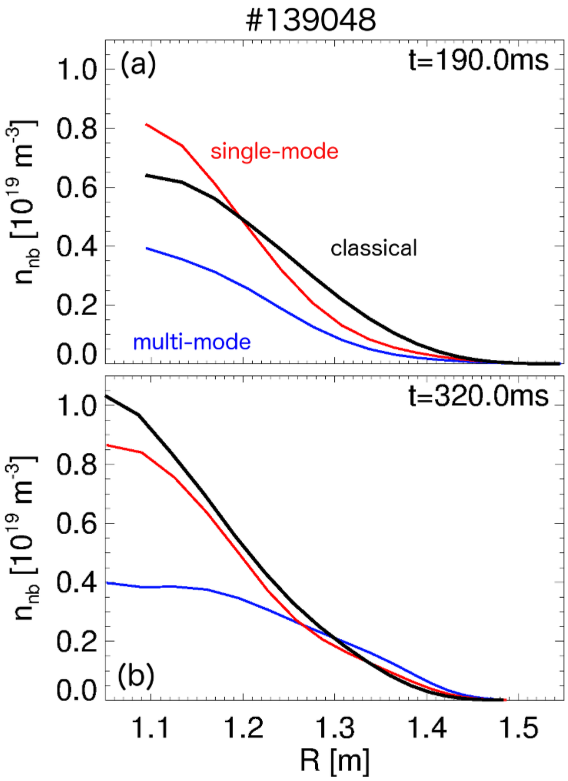

FIG. 11: Fast ion density profile at two different times from multi- vs single-mode simulations, cf. Fig. 10b. Note the steepening of the density at $t \approx 190$ ms for the single-mode case, which indicates inconsistency of the assumptions on mode amplitude at that time if all other modes are removed from the simulation.

port models have been compared for a NSTX discharge featuring robust Alfvénic activity. It is concluded that retaining phase space effects does indeed lead to significant variations in the EP distribution and its temporal evolution, which are not captured by simple diffusive models.

Effects of the distortion of the EP distribution can propagate to integral quantities such as radial EP density, loss rate and power damped to the plasma through thermalization. Although the radial profile of those quantities is quite model-dependent, differences between the two models eventually reduce as further integrations over minor radius are performed, e.g. to compute the total neutron rate or stored energy.

Clearly, more sophisticated transport models, such as the kick model discussed herein, can provide valuable information to assess the consistency of the simulations. For example, the computed power exchanged between fast ions and instabilities can be used as an indicator to verify the initial assumptions on the modes responsible for enhanced EP transport and the overall consistency of the simulations.

The improved treatment of EP transport by instabilities can make integrated simulations more reliable, at the expenses of increased complexity of the underlying analysis of instabilities and their stability properties. The final choice between EP transport models used in the simulations should therefore be based on the expectations for simulation's output - in short, whether *global* performance indicators (e.g. neutron rate, stored energy or overall NB-CD efficiency) or more details on quantities such as EP distribution function and/or radial profiles EP-related quantities are required.

Acknowledgments

This material is based upon work supported by the U.S. Department of Energy, Office of Science, Office of Fusion Energy Sciences under contract number DE-AC02-09CH11466. NSTX at Princeton Plasma Physics Laboratory is a DOE Office of Science User Facility. The digital data for this paper can be found in http://arks.princeton.edu/ark:/88435/dsp018p58pg29j.

[1] A. Fasoli, C. Gormezano, H. L. Berk, B. N. Breizman, S. Briguglio, D. S. Darrow, N. N. Gorelenkov, W. W. Heidbrink, A. Jaun, S. V. Konovalov, R. Nazikian, J.-M. Noterdaeme, S. Sharapov, K. Shinoara, D. Testa, K. Tobita, Y. Todo, G. Vlad, and F. Zonca, Nucl. Fusion **47**, S264 (2007)
[2] W. W. Heidbrink and G. J. Sadler, Nucl. Fusion **35**, 243 (1995)
[3] N. N. Gorelenkov, S. D. Pinches, and K. Toi, Nucl. Fusion **54**, 125001 (2014)
[4] D. A. Spong, B. A. Carreras, and C. L. Hedrick, Phys. Fluids B **4**, 3316 (1992)
[5] S. Briguglio, G. Vlad, F. Zonca, and C. Kar, Phys. Plasmas **2**, 3711 (1995)
[6] W. Park, E. V. Belova, G. Y. Fu, X. Z. Tang, H. R. Strauss, and L. E. Sugiyama, Phys. Plasmas **6**, 1796 (1999)
[7] J. Lang, Y. Chen, S. E. Parker, and G. Fu, Phys. Plasmas **16**, 102101 (2009)
[8] Y. Todo, K. Shinohara, M. Takechi, and M. Ishikawa, Phys. Plasmas **12**, 012503 (2005)
[9] M. Schneller, P. Lauber, R. Bilato, M. Garcia-Munoz, M. Brudgam, S. Gunter, and the ASDEX Upgrade Team, Nucl. Fusion **53**, 123003 (2013)
[10] K. Ghantous, N. N. Gorelenkov, H. L. Berk, W. W. Heidbrink, and M. A. Van Zeeland, Phys. Plasmas **19**, 092511 (2012)
[11] W. W. Heidbrink, M. A. Van Zeeland, M. E. Austin, E. M. Bass, K. Ghantous, N. N. Gorelenkov, B. A. Grierson, D. A. Spong, and B. J. Tobias, Nucl. Fusion **53**, 093006 (2013)
[12] R. E. Waltz and E. M. Bass, in 13th IAEA-TM EP meeting (Beijing, China, 2013)
[13] N. N. Gorelenkov, W. W. Heidbrink,

G. J. Kramer, J. Lestz, M. Podestà, M. A. Van Zeeland, and R. B. White, in 14th IAEA Technical Meeting on Energetic Particles in magnetic confinement systems, O-06 (Vienna, Austria, 2015)

[14] M. Ono, S. M. Kaye, Y.-K. M. Peng, G. Barnes, W. Blanchard, M. D. Carter, J. Chrzanowski, L. Dudek, R. Ewig, D. Gates, R. E. Hatcher, T. Jarboe, S. C. Jardin, D. Johnson, R. Kaita, M. Kalish, C. E. Kessel, H. Kugel, R. Maingi, R. Majeski, J. Manickam, B. McCormack, J. Menard, D. Mueller, B. Nelson, B. Nelson, C. Neumeyer, G. Oliaro, F. Paoletti, R. Parsells, E. Perry, N. Pomphrey, S. Ramakrishnan, R. Raman, G. Rewoldt, J. Robinson, A. L. Roquemore, P. Ryan, S. Sabbagh, D. Swain, E. J. Synakowski, M. Viola, M. Williams, J. R. Wilson, and NSTX Team, Nucl. Fusion **40**, 557 (2000)

[15] J. E. Menard, S. Gerhardt, M. Bell, J. Bialek, A. Brooks, J. Canik, J. Chrzanowski, M. Denault, L. Dudek, D. A. Gates, N. Gorelenkov, W. Guttenfelder, R. Hatcher, J. Hosea, R. Kaita, S. Kaye, C. Kessel, E. Kolemen, H. Kugel, R. Maingi, M. Mardenfeld, D. Mueller, B. Nelson, C. Neumeyer, M. Ono, E. Perry, R. Ramakrishnan, R. Raman, Y. Ren, S. Sabbagh, M. Smith, V. Soukhanovskii, T. Stevenson, R. Strykowsky, D. Stutman, G. Taylor, P. Titus, K. Tresemer, K. Tritz, M. Viola, M. Williams, R. Woolley, H. Yuh, H. Zhang, Y. Zhai, A. Zolfaghari, and NSTX Team, Nucl. Fusion **52**, 083015 (2012)

[16] R. Hawryluk, in Physics of plasmas close to thermonuclear conditions (Proceedings from the International School of Plasma Physics, 1979, Villa Monastero, Varenna - Italy, 1979)

[17] For more details on the TRANSP code, please visit the TRANSP webpage at http://w3.pppl.gov/~pshare/help/transp.htm

[18] R. J. Goldston, D. C. McCune, H. H. Towner, S. L. Davis, R. J. Hawryluk, and G. L. Schmidt, J. Comput. Phys. **43**, 61 (1981)

[19] A. Pankin, D. McCune, R. Andre, G. Bateman, and A. Kritz, Computer Physics Communication **159**, 157 (2004)

[20] M. Podestà, M. Gorelenkova, and R. B. White, Plasma Phys. Control. Fusion **56**, 055003 (2014)

[21] R. B. White and M. S. Chance, Phys. Fluids **27**, 2455 (1984)

[22] C. Z. Cheng, Phys. Rep. 211 **1** (1992)

[23] G. Y. Fu, C. Z. Cheng, and K. L. Wong, Phys. Fluids B **5**, 4040 (1993)

[24] N. N. Gorelenkov, C. Z. Cheng, and G. Y. Fu, Phys. Plasmas **6**, 2802 (1999)

[25] R. B. White, The theory of toroidally confined plasmas, 3rd ed. (Imperial College Press, London, UK, 2014)

[26] S. S. Medley and A. L. Roquemore, Rev. Sci. Instr. **75**, 3625 (2004)

[27] S. Kubota, X. V. Nguyen, W. A. Peebles, L. Zeng, and E. J. Doyle, Rev. Sci. Instr. **72**, 348 (2001)

[28] N. A. Crocker and W. A. Peebles and S. Kubota and J. Zhang and R. E. Bell and E. D. Fredrickson and N. N. Gorelenkov and B. P. LeBlanc and J. E. Menard and M. Podestà and S. A. Sabbagh and K. Tritz and H. Yuh, Plasma Phys. Control. Fusion **53**, 105001 (2011)

[29] E. D. Fredrickson, N. A. Crocker, R. E. Bell, D. S. Darrow, N. N. Gorelenkov, G. J. Kramer, S. Kubota, F. M. Levinton, D. Liu, S. S. Medley, M. Podestà, K. Tritz, R. B. White, and H. Yuh, Phys. Plasmas **16**, 122505 (2009)

[30] E. D. Fredrickson, N. A. Crocker, D. S. Darrow, N. N. Gorelenkov, G. J. Kramer, S. Kubota, M. Podestà, R. B. White, A. Bortolon, S. P. Gerhardt, R. E. Bell, A. Diallo, B. P. LeBlanc, F. M. Levinton, and H. Yuh, Nucl. Fusion **53**, 013006 (2013)

[31] E. M. Carolipio, W. W. Heidbrink, C. B. Forest, and R. B. White, Nucl. Fusion **42**, 853 (2002)

[32] R. B. White, N. N. Gorelenkov, W. W. Heidbrink, and M. A. V. Zeeland, Plasma Phys. Control. Fusion **52**, 045012 (2010)

[33] M. Podestà, M. Gorelenkova, E. D. Fredrickson, N. N. Gorelenkov, and R. B. White, Nucl. Fusion(submitted, 2015)

Princeton Plasma Physics Laboratory
Office of Reports and Publications

Managed by
Princeton University

under contract with the
U.S. Department of Energy
(DE-AC02-09CH11466)

P.O. Box 451, Princeton, NJ 08543
Phone: 609-243-2245
Fax: 609-243-2751

E-mail: publications@pppl.gov

Website: http://www.pppl.gov